IMR&D

IMRD 是學術論文的基本架構，意指 Introduction/Method/Results/Discussion，是論文的論證策略結構，通常還須加上 Reference。

請從以下論文 Abstract，找出摘要包含的主要部分，並說明學術論文中「摘要」的論證流程。

請說明 introduction 在論文中的角色及功能。

請說明 method 當中 theory 或 experimental setup 在論文中的角色及功能。

請說明 results 在論文中的角色及功能。

請說明 discussion 在論文中的角色及功能。

請說明 reference 在論文中的角色及功能，從科學論證的角度思考引用論文[*]的用意。

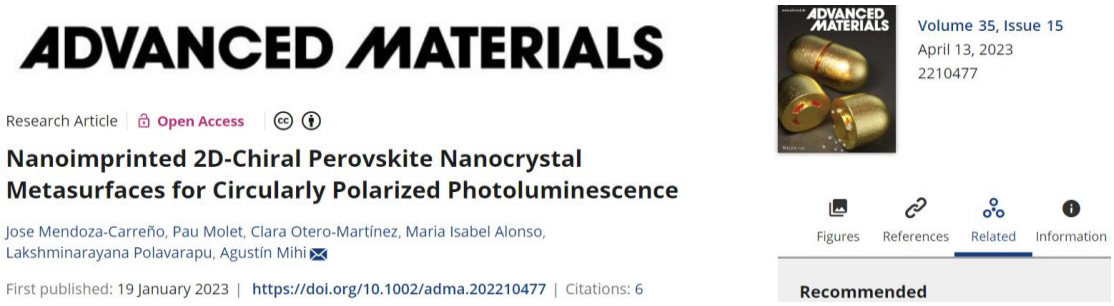

Nanoimprinted 2D-Chiral Perovskite Nanocrystal Metasurfaces for Circularly Polarized Photoluminescence

Jose Mendoza-Carreño, Pau Molet, Clara Otero-Martínez, Maria Isabel Alonso, Lakshminarayana Polavarapu, Agustín Mihi*

Corresponding author: amihi@icmab.es

Abstract

The versatile hybrid perovskite nanocrystals (NCs) are one of the most promising materials for optoelectronics by virtue of their tunable bandgaps and high photoluminescence (PL) quantum yields. However, their inherent crystalline chemical structure limits the chiroptical properties achievable with the material. The production of chiral perovskites has become an active field of research for its promising applications in optics, chemistry, or biology. Typically, chiral halide perovskites are obtained by the incorporation of different chiral moieties in the material. Unfortunately, these chemically modified perovskites have demonstrated moderate values of chiral PL so far. Here, a general and scalable approach is introduced to produce chiral PL from arbitrary nanoemitters assembled into 2D-chiral metasurfaces. The fabrication via nanoimprinting lithography employs elastomeric molds engraved with chiral motifs covering millimeter areas that are used to pattern two types of unmodified colloidal perovskite NC inks: green-emissive CsPbBr3 and red-emissive CsPbBr1I2. The perovskite 2D-metasurfaces exhibit remarkable PL dissymmetry factors (glum) of 0.16 that can be further improved up to glum of 0.3 by adding a high-refractive-index coating on the metasurfaces. This scalable approach to produce chiral photoluminescent thin films paves the way for the seamless production of bright chiral light sources for upcoming optoelectronic applications.

1 Introduction

Circularly polarized (CP) light is used in a vast number of photonic technologies, including 3D-imaging,[1, 2] biosensing,[3, 4] bioimaging,[5] photocatalysts for asymmetrical synthesis,[6, 7] encrypted transmission,[8] and spintronics,[9] photoelectric devices, and chiroptical materials. Traditionally, CP light

is produced from unpolarized light by a combination of linear polarizers and quarter wave-plates or phase-shifting mirrors. These optical components limit device miniaturization, high-speed operation, and cause severe brightness losses due to undesired light trapping. Said limitations can be overcome with the use of luminescent chiral materials. Unfortunately, chiral light emitters are very scarce in nature and resorting to chemical modification of existing luminescent materials is a challenging task that has resulted in limited fractions of circularly polarized luminescence (CPL) so far.[10]

Over the last few years, halide perovskite nanocrystals (NCs) have emerged as one of the most efficient materials for optoelectronics because of a high photoluminescence (PL) quantum yield, tunable emission across the entire visible spectrum, and highly scalable colloidal synthesis.[11-13] The defect-tolerant nature of bromide and iodide halide perovskites enables the high PL quantum yield without the need of high bandgap passivation shells on their surfaces.[14, 15] The ambitious next step in the development of metal halide perovskites is to endow them with chiral properties.[16] To this end, the synthetic versatility of metal halide perovskites is exploited for the incorporation of chiral organic molecules, either a bulky organic chiral cation inside the perovskite structure,[17] a chiral molecule embedded between the layers of 2D-perovskites,[9, 18, 19] or a chiral capping ligand in NCs.[20] Despite great efforts, chemical modification has provided limited values of CPL[21] at room temperature with glum values on the order of 10−3 which are insufficient for practical applications.[21]

2 Results and Discussion

Two types of perovskite nanocube inks (CsPbBr3 and CsPbBr1I2 NCs) were synthesized by ligand-assisted tip-ultrasonication and halide exchange (Figure S2, Supporting Information). The CsPbBr3 NCs, exhibit green PL with a peak maximum at 519 nm (Figure 1a), while the CsPbBr1I2 NCs emit red PL with a peak maximum at 645 nm (Figure 1b).

The CPL-active chiral nanostructures were fabricated via template-induced self-assembly of halide perovskite NC inks using three different pre-patterned poly(dimethylsiloxane) (PDMS) molds with 500 nm gammadion-like structures (9 mm2 patterned areas) with left (L), right (R), and racemic (O) orientations in a square array with a periodicity of 600 nm (structure dimensions in Figure 1c).

The fabrication process, summarized in Figure 1d, begins with 0.7 µL of the colloidal solution deposited on a cleaned glass coverslip and immediately covered with the pre-patterned stamp.

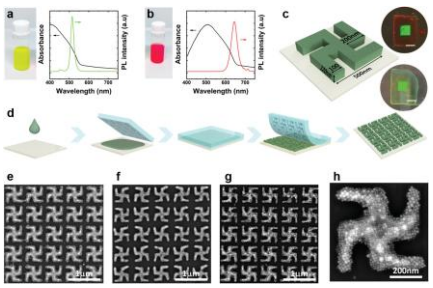

Figure 1

Fabrication of the 2D-chiral metasurface. Photograph of the original colloidal dispersion, extinction, and PL intensity spectra of green CsPbBr3 NCs (a) and red CsPbBr1I2 NCs (b). c) Schematic of the chiral unit. Inset photographs of the actual samples of red CsPbBr1I2 NCs (top) and green CsPbBr3 NCs (bottom) large area 2D-chiral metasurfaces with a scale bar = 3 mm. d) Schematic

illustration of the fabrication process of 2D-chiral metasurfaces by the templated-assembly technique. e–g) SEM images of L-gammadion (e), O-racemic (f), and R-gammadion (g) metasurfaces. h) Large-magnification SEM of an L-gammadion unit composed by CsPbBr3 perovskite NCs.

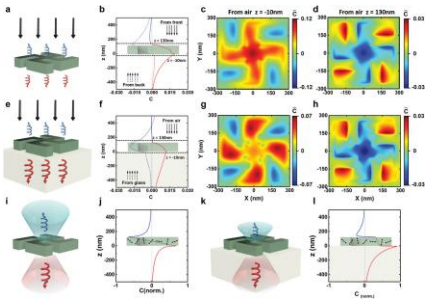

Figure 2

Optical chirality C inversion and dissymmetry for both sides of L-gammadion at the emission wavelength (520 nm). a,b,e,f) Schematic illustrations of an L-gammadion transferring optical chirality to unpolarized light and the calculated optical chirality factor along the propagation axis for a system with (first row) (a,b) and without (second row) (e,f) inversion symmetry along the axis. c,d,g,h,) Local optical chirality factor in the symmetric and non-symmetric system at 10 nm distance from the gammadion unit for the transmitted (z = 130 nm) (c,g) and reflected (z = −10 nm) (d,h) light. i,k) Schematic illustration of an L-gammadion emitting both polarizations for a system with (i) and without (k) inversion symmetry along the axis depending on the surface of emission measurement. j,l) Normalized optical chirality factor computed by FDTD simulations for randomly out of phase dipole cloud placed within the L-gammadion volume polarizations for a system with (j) and without (l) inversion symmetry

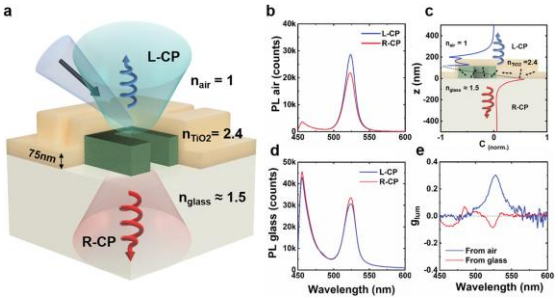

Figure 4

Chiral dissymmetry PL emission from the 2D-chiral metasurface coated with 75 nm of TiO2. a) Schematic illustration for the excitation of a high refractive index TiO2 coated L-gammadion emitting preferentially L- or R-PL on each side of the metasurface. b,d) Chiral PL measurement of L-CP (blue) and R-CP (red) measured from the air (b) and glass (d) sides. c) Normalized optical chirality factor computed by FDTD simulations for a randomly out-of-phase dipole cloud placed within perovskite L-gammadion volume. e) Comparison of the glum measured through the air (blue) and the glass (red) side.

3 Conclusions

We have demonstrated large area CPL-active halide perovskite NCs chiral structures using template-induced self-assembly. We produced 2D-chiral metasurfaces by nanostructuring two types of non-chiral halide perovskite NCs, CsPbBr3 and CsPbBr1I2 into gammadion arrays. This low cost and scalable fabrication approach can be seamlessly applied to other kind of emitters, including those with intrinsic chirality, to directly obtain circularly polarized light with relevant glum values. In this work, the fabricated 2D-chiral

metasurfaces rendered the perovskite NCs with CPL selectivities reaching glum values up to 0.16 at RT. Opposed handedness CPL is observed at each side of the 2D chiral metasurface, which is corroborated numerically by analyzing the optical chirality of the near-fields generated at top and bottom sides of the structure in air or glass supported. Finally, we further improved the chiral emission properties of the metasurface by adding a thin film of a transparent high-refractive-index material atop. This coating rendered maximum glum factors of 0.31 and demonstrated the ability to design and optimize the preferential chiral response by engineering the layers composing the metasurface. We believe that the work presented herein will contribute to the development of large scale selective CPL sources with the most efficient common light emitters that can be combined with chemical modification to achieve even greater CPL values with great potential for displays and quantum technologies.

4 Experimental Section

Materials

Cesium carbonate (Cs2CO3, 99.9%), lead (II) bromide (PbBr2, >98%), lead (II) iodide (PbI2, 99%), 1-octadecene (C18H36, 90%), oleic acid (C18H34O2, 90%), and oleylamine (C18H37N, 70%) were purchased from Merck. Hellmanex III solution and hexane solutions were purchased from Millipore-Sigma. Acetone, isopropanol, and NaOH were purchased from Labbox. PDMS (Sylgard 184) was purchased from Dow Corning (Michigan, USA). The hard PDMS (hPDMS) mixture kit was purchased from Gelest (USA). All chemicals were used as received.

Preparation of the Patterned Stamps

Preparation of the Original Master Structures: The original silicon masters (purchased from CONSCIENCE, Sweden) were constituted of arrays of gammadion shapes with 500 nm width and 120 nm depth, disposed in a squared arrangement forming a lattice of 600 nm pitch in 3 × 3 mm2 areas. The masters were silanized with an anti-sticking layer of perfluorooctyl–trichlorosilane to prevent the adhesion of the silicones and resistance during replication. The silanization took place through chemical vapor deposition, leaving the masters for 30 min in a desiccator under vacuum together with 4 µL of perfluorooctyl–trichlorosilane. The substrates were rinsed with acetone and heated to 150 °C for 30 min to remove unreacted silane.

Optical Characterization

UV–Vis and Photoluminescence Spectroscopy: UV–vis extinction spectra were obtained using a Cary-60 UV–vis spectrophotometer (Agilent). PL spectra were obtained with a Cary Eclipse Fluorescence Spectrophotometer (Agilent). Quartz cuvettes with an optical path length of 1 cm were used for both optical analyses.

Ellipsometry: The optical constants of the perovskites were determined from measurements using a GES5E ellipsometer from SOPRALAB with a spectral range from 1.2 to 5.5 eV. All regression analyses were performed using an in-house code.

Transmittance Circular Dichroism: The optical measurements were carried out in a custom-made optical set

up. A white tungsten halogen lamp (Ocean Optics, HL-2000-HP, FL, USA) corrected with two filters in the UV and NIR (Edmund Optics, SCHOTT BG64, and Thorlabs, SRF11) was coupled to protected silver reflective collimator (RC08SMA-P01, Thorlabs) as light source injection. The light collection consisted of another protected silver reflective collimator coupled to a spectrometer (Ocean Optics, QEPro-FL) by an optical fiber. The collimated white light beam was sent through a Glan-Thompson Calcite Polarizer (GTH10M, Thorlabs) mounted on a stepper motor rotation mount (K10CR1/M, Thorlabs). The linearly polarized light obtained was directed to a super achromatic quarter wave-plate (SAQWP05M-700, Thorlabs) mounted at $\pm\pi/4$ compared to the polarization direction on a rotation mount (ELL14, Thorlabs) to obtain a circularly polarized light beam. All the optical elements were controlled automatically by custom software (LabView NXG) to ensure the reproducibility of the measurements. The illumination area was controlled by a pinhole (SM1D12). Two dual-position sliders (ELL6, Thorlabs) were used to place a shutter and the sample in the beam path. The first one was used to measure the dark current of the spectrometer, whereas the second one was used to place the sample in the light beam. The sample was placed between a pair of 4× objectives (NA = 0.1).

Chiral Emission Characterization: Two laser sources (NPL41B, Thorlabs and Crylas FDSS 532-150) with peak emission at 405 and 532 nm were used to excite $CsPbBr_3$ and $CsPbBr_1I_2$ NCs, respectively. The PL obtained from the samples was collected through a 4× objective with 0.1 NA and collimated to a super achromatic quarter-wave plate and a Glan-Thomson polarizer. By means of a trigger controlled externally by an Arduino board (Arduino Uno), a fixed number of laser pulses were sent onto the sample to ensure both polarizations were given the same amount of energy in the excitation process. The laser signals were optically filtered using longpass band filters (FELH0450, Thorlabs for 405 nm laser, BLP01-532R-25, Semrock for the 532 nm laser line).

FDTD Simulations

General Considerations: FDTD simulations were performed using a commercial software (Lumerical Inc. by Ansys). The simulation reproduced a single 120 nm height and 500 nm-long gammadion-like structure with 100 nm arms (width) composed of a material whose optical parameters were obtained from ellipsometry measurements (Figure S8, Supporting Information) for each type of perovskite NCs. Perfectly matched layers (PMLs) were set in all x, y, and z directions. In the case of the z-direction, the PML was placed at a z that was at least half of the maximum wavelength ensure the absorption of the light source in the propagation axis avoiding back reflections and interference in the simulation region. The same PML boundary conditions were used in the x and y directions for unpolarized excitation and dipole clouds simulations.

Transmittance Characterization: Two orthogonal plane wave sources with a spectral range in the visible–NIR in the x and y direction with a phase difference of $\pm\pi/2$ were used as R-CP and L-CP input light. A pair of 2D z-normal power monitors were placed to measure the transmittance and reflectance spectra for both polarizations. In the x and y directions, periodic boundary conditions were used to simulate the 2D-chiral photonic metasurface.

Reference

[1] N. Ji, K. Zhang, H. Yang, Y.-R. Shen, J. Am. Chem. Soc. 2006, 128, 3482.

[2] A. N. Simonov, M. C. Rombach, Opt. Lett. 2011, 36, 115.

[3] X. Wu, L. Xu, L. Liu, W. Ma, H. Yin, H. Kuang, L. Wang, C. Xu, N. A. Kotov, J. Am. Chem. Soc. 2013, 135, 18629.

[4] M. L. Solomon et al., Acc. Chem. Res. 2020, 53, 588.

[5] S. Lee, Y. Sun, Y. Cao, S. H. Kang, Trends Analyt Chem 2019, 117, 58.

[6] X. Liu, Y. Lin, Y. Liao, J. Wu, Y. Zheng, J. Mater. Chem. C 2018, 6, 3499.

[7] X. Wei, J. Liu, G.-J. Xia, J. Deng, P. Sun, J. J. Chruma, W. Wu, C. Yang, Y.-G. Wang, Z. Huang, Nat. Chem. 2020, 12, 551.

[8] C. Li, X. Yang, J. Han, W. Sun, P. Duan, Mater. Adv. 2021, 2, 3851.

[9] G. Long et al., Nat. Photonics 2018, 12, 528.

[10] Y. Sang, J. Han, T. Zhao, P. Duan, M. Liu, Adv. Mater. 2020, 32, 1900110.

[11] L. Protesescu et al., Nano Lett. 2015, 15, 3692.

[12] Y. Tong et al., Angew. Chem., Int. Ed. 2016, 55, 13887.

[13] J. Shamsi, A. S. Urban, M. Imran, L. De Trizio, L. Manna, Chem. Rev. 2019, 119, 3296.

[14] J. Ye, M. M. Byranvand, C. O. Martínez, R. L. Z. Hoye, M. Saliba, L. Polavarapu, Angew. Chem. 2021, 133, 21804.

[15] A. Dey et al., ACS Nano 2021, 15, 10775.

[16] G. Long et al., Nat. Rev. Mater. 2020, 5, 423..

[17] D. Di Nuzzo, L. Cui, J. L. Greenfield, B. Zhao, R. H. Friend, S. C. J. Meskers, ACS Nano 2020, 14, 7610.

[18] J. Ma, C. Fang, C. Chen, L. Jin, J. Wang, S. Wang, J. Tang, D. Li, ACS Nano 2019, 13, 3659.

[19] Y. Liu et al., J. Mater. Chem. C 2020, 8, 5673.

[20] Z. N. Georgieva, B. P. Bloom, S. Ghosh, D. H. Waldeck, Adv. Mater. 2018, 30, 1800097.

[21] J. Ma, H. Wang, D. Li, Adv. Mater. 2021, 33, 2008785.